JOURNAL OF MATERIALS SCIENCE **36** (2001) 113–122

Atomic force microscopy, a powerful tool to study blend morphologies based on polyester resins

C. SERRÉ, M. VAYER, R. ERRE
Centre de Recherche sur la Matière Divisée CNRS- Université d'Orléans, 1b rue de la Férollerie F45071 Orléans Cedex 2
E-mail: marylene.vayer@univ-orleans.fr

N. BOYARD, C. OLLIVE
Menzolit Z.I. BP 19, F41353 Vineuil Cedex

Atomic Force Microscopy (AFM) was an unusual but effective tool used to investigate the morphology of cured blends based on UP (unsaturated polyester). The pertinence of AFM was evaluated by studying four miscible UP/LPA (low profile additive)/ST (styrene) blend systems. The morphology of these cured blends before and after LPA solubilization was analogous in SEM (Scanning Electron Microscopy) and AFM. However, in AFM the particles boundaries were more defined compared to SEM. Before treatment, nanoparticles (less than 60 nm) and aggregates (140 to 250 nm) were discernible. After treatment, nanogels (less than 50 nm) and microgels (80 to 220 nm) were observed. The aggregates composed of linked nanoparticles, were connected together to form a whole network. The microgels were composed of linked nanogels and were connected to form a polyester network. The LPA solubilization reduced the nanoparticles to nanogels in extracting the LPA phase out of the nanoparticles. The particles size depended on the miscibility of the system UP/LPA/ST and was related to the void volume. Shrinkage and light opacity were macroscopic properties which characterized the void volume and therefore the particle sizes.

1. Introduction

Unsaturated polyester (UP) resin (60 wt %), vinyl monomer (40 wt %) - usually styrene (ST) - and low profile additive (LPA) such as thermoplastic polymer like poly(vinylacetate) (PVAc) [1–11] poly(methyl methacrylate) (PMMA) [1, 3–6, 12], polyurethane (PU) [1, 5, 6] and polystyrene (PS) [1, 5, 6] generally composed the most studied thermoset blends. The thermal expansion of LPA compensates for the polymerization shrinkage of the UP/ST and the LPA does not participate in the polymerization process [11].

The morphology of blends UP/LPA/ST after curing depends on the initial UP/LPA/ST ternary system miscibility at room temperature [6, 7] and on the phase separation between UP, LPA and ST [8] during curing. Both of these parameters depend upon the chemical nature, dipole moment [6], glass transition temperature and molecular weight of the components [6, 13].

Miscible systems are the most investigated systems. During curing the free-radical chain-growth copolymerization between the styrene and UP molecules [14, 15] increases the molecular weight of these crosslinked molecules [2]. LPA and the crosslinked molecules become non-miscible and lead to phase separation with the apparition of particles. The morphology of the cured blends is determined by the competition between the crosslinking kinetic and the ongoing kinetic of the phase separation [3]. When the system is totally miscible, this morphology is described as a co-continuous structure with a phase of connected microgels in a network and a continuous phase of LPA surrounding the microgels [4]. Microvoids are created inside this LPA phase or/and at the interface between LPA and UP phases [5, 6, 11, 12], indicating that LPA reduces polymerization shrinkage.

Most work explores only the microgel networks. Indeed, optical microscopy [1, 9, 12, 14, 16] and more recently, Scanning Electron Microscopy (SEM) [2–7, 10, 14, 15] have been used to investigate cured samples after solubilization of the non-polymerized products (especially the LPA). Microgel networks were seen to vary from a flake-like structure to a coral-like structure [15]. The ST percentage, the nature of LPA and UP influence microgel particle sizes between 0.2 and 8 μm [2, 6, 16]. Few work shows the whole morphology within a microgel network and a LPA phase [4].

AFM technique has been successfully used to characterize topography at the nanometric scale of many surfaces of advanced materials (coatings, thin films, paints, biological samples) and allows direct observation of some surface processes (eg. corrosion) [17]. The present work evaluated the capability of AFM to provide pertinent information on the morphology of cured blends. To achieve this goal, we studied cured samples

of miscible systems UP/LPA/ST by Scanning Electron Microscopy (SEM) and by Atomic Force Microscopy (AFM). The samples were observed either before or after treatment to solubilize non-polymerized products. Consequently, we respectively investigated whole morphology and the microgel networks.

2. Experimental

2.1. Materials

UP and LPA resins were respectively named UPST-N, UPST-P and LPAST-U, LPAST-A. Their characteristics are reported in Table I. Four blends were prepared by mixing UPST-N/LPAST-U, UPST-N/LPAST-A, UPST-P/LPAST-U and UPST-P/LPAST-A in a weight proportion of 69 : 30. No additional styrene was added. The reaction was initiated by 1 wt % of t-butyl ethyl-2 perhexanoate (TBPEH). The UP/LPA/ST weight composition was 46 : 12 : 41.

2.2. Instrumentation

SEM (Scanning Electron Microscopy) was carried out on a HITACHI S 4200 device combined with an OXFORD Analyzer controlled by LINK ISIS software. SEM was operated at 5 keV. At this accelerated voltage, secondary electrons were collected over a depth of 150 nm [18, 19]. The theoretical resolution of SEM microscope, given by the Abbe formula, was estimated in our case to be 2 nm ($\alpha = 5 \times 10^{-3}$ rd). The experimental resolution also depended upon the sample nature (electronic conductivity and roughness).

AFM (Atomic Force Microscopy) measurements were carried out in air using Nanoscope III software from Digital Instruments Corporation in the tapping

TABLE I UPST and LPAST characteristics: type of product, styrene wt % and viscosity $\eta_{(Po)}$

Name	Type of product	Styrene (wt %)	$\eta_{(Po)}$
UPST-N	PG-NPG maleate resin	33	15
UPST-P	PG maleate resin	34	20
LPAST-U	urethane modified polyester diol	60	2
LPAST-A	saturated polyester based on adipic acid	60	0,5

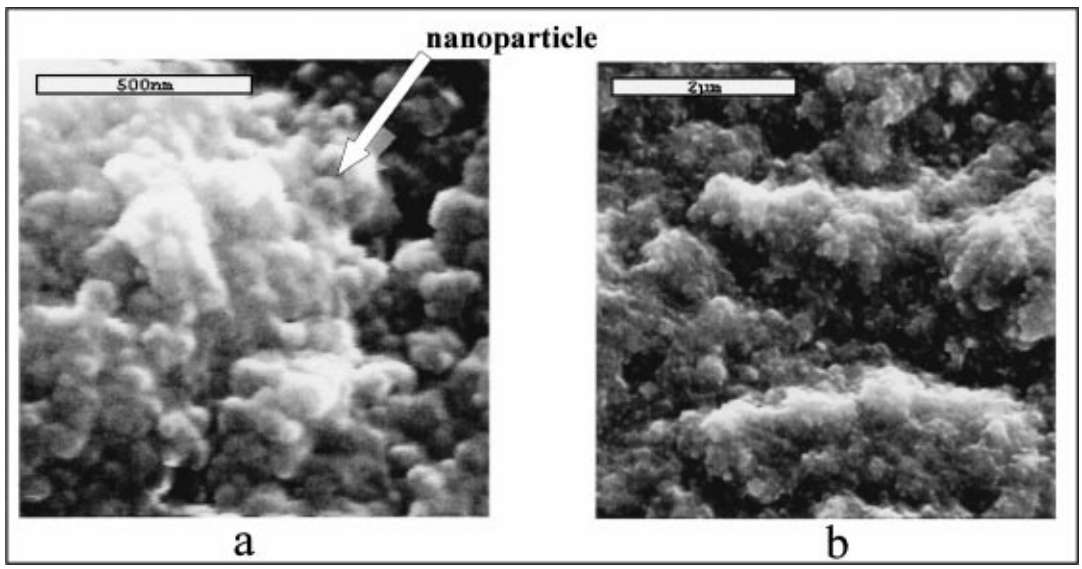

Figure 1 UPST-N/LPAST-A fractured surfaces by SEM before treatment (a) 1 μm × 1 μm (b) 5 μm × 5 μm.

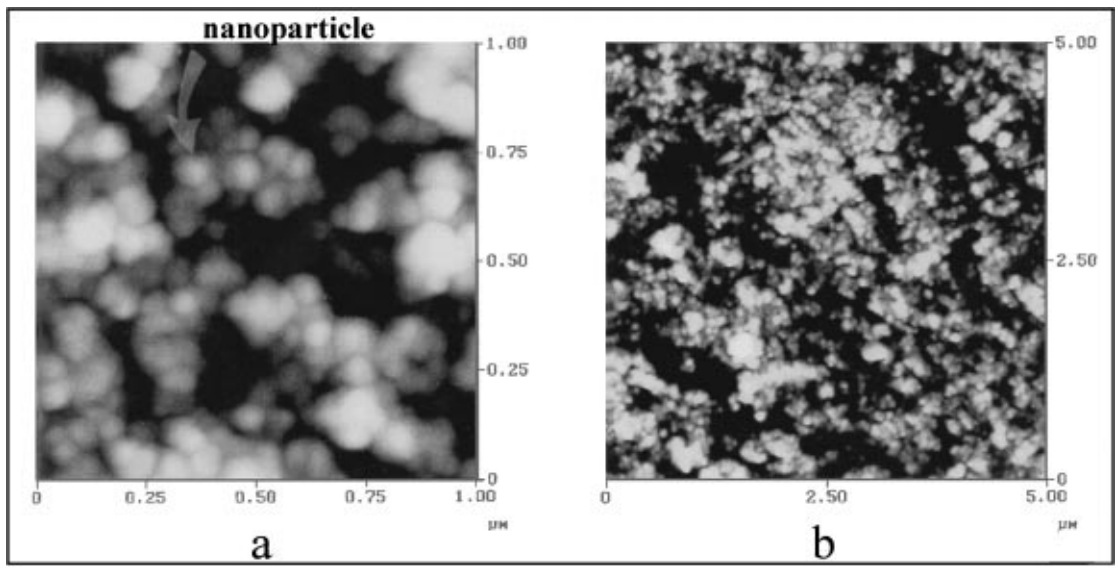

Figure 2 UPST-N/LPAST-A fractured surfaces by AFM before treatment (a) 1 μm × 1 μm, z range = 100 nm (b) 5 μm × 5 μm, z range = 100 nm.

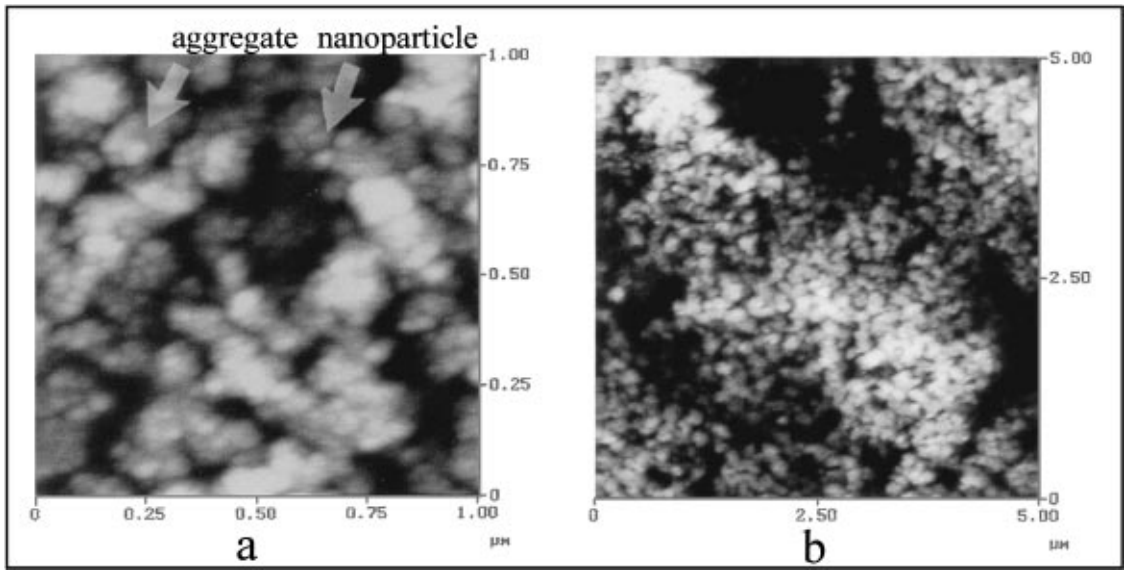

Figure 3 UPST-N/LPAST-A surfaces by AFM before treatment (a) 1 μm $\times$ 1 μm, z range = 50 nm (b) 5 μm $\times$ 5 μm, z range = 80 nm.

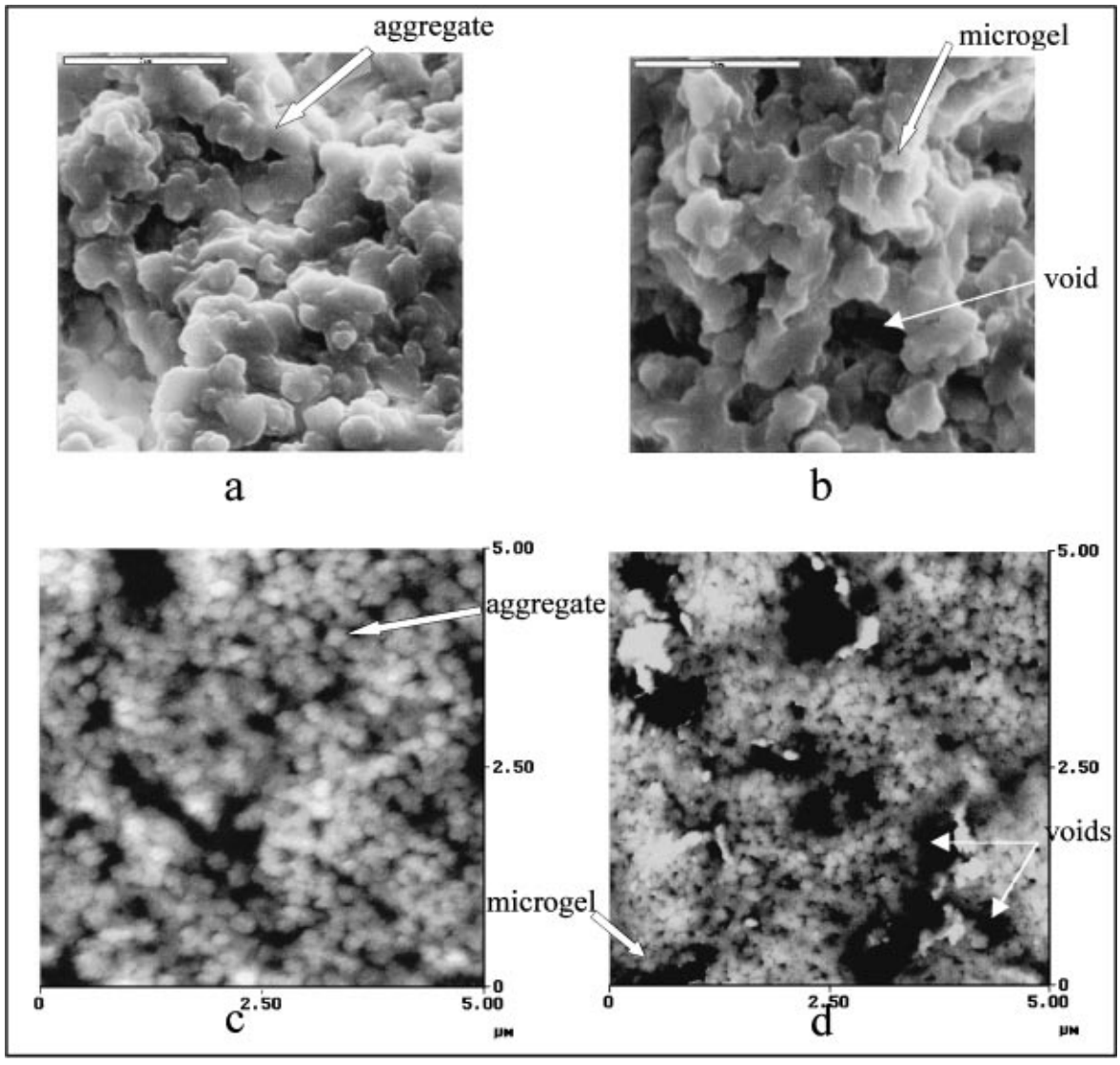

Figure 4 UPST-P/LPAST-U sample before treatment (a) fractured surface by SEM, 5 μm $\times$ 5 μm (c) surface by AFM, 5 μm $\times$ 5 μm, z range = 80 nm; after treatment (b) fractured surface by SEM, 5 μm $\times$ 5 μm (d) surface by AFM, 5 μm $\times$ 5 μm, z range = 80 nm.

mode. The piezo scanner was able to scan with a horizontal range of 150 μm and a vertical range of 7 μm. Microfabricated Si cantilevers, with a cantilever length of 120 μm, with integrated Si pyramidal tip (10 to 15 μm height) were used. The resonance frequency was 200–400 kHz. The vertical and lateral resolutions were less than 1 nm.

2.3. Procedure

UPST/LPAST blends were cured using a Derek press in a stainless steel mold coated by a protective film, at 100 bars for 300 seconds (∅ 50 mm, thickness 4 mm). The temperature was raised to 150 °C at the female part and 135 °C at the punching die side.

Cured samples were broken into several pieces. Some pieces were soaked in dichloromethane (CH_2Cl_2) for two hours to remove non-crosslinked soluble material (unreacted ST, LPA). This method is called treatment in the present paper.

For SEM observations, samples were carbon coated to render them conductive and were degassed under vacuum conditions before examination.

AFM did not require any specific preparation. However, observations had to be performed on the flattest possible regions.

The size of images in AFM varied from 1×1 μm^2 to 10×10 μm^2 with 512×512 pixels and in SEM from 1×1 μm^2 to 5×5 μm^2 with 384×384 pixels. The pixel size limited lateral image resolution: this is displayed in Table II.

The average particle sizes and void volumes were measured by means of AFM image analysis. The volume shrinkages were estimated by varying the diameters and the thicknesses of samples.

TABLE II Pixel sizes of SEM and AFM images

Scan size (μm^2)	1×1	2×2	5×5	10×10
size of one pixel by AFM (nm^2)	2×2	4×4	10×90	20×20
size of one pixel by SEM (nm^2)	3×3	5×5	13×13	26×26

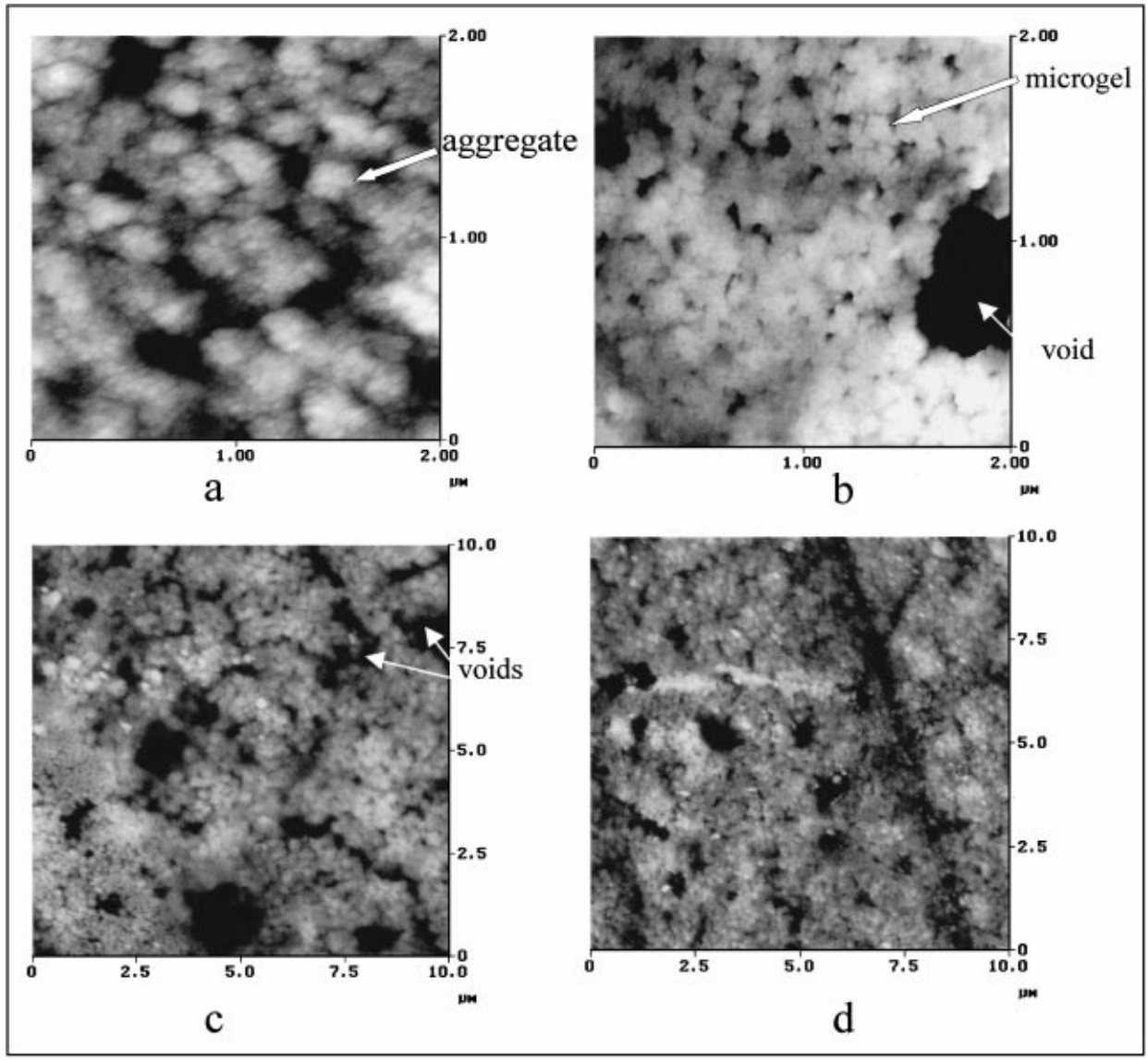

Figure 5 UPST-P/LPAST-U surfaces by AFM, before treatment (a) 2 μm × 2 μm, z range = 50 nm (c) 10 μm × 10 μm, z range = 80 nm; after treatment (b) 2 μm × 2 μm, z range = 100 nm (d) 10 μm × 10 μm, z range = 100 nm.

Several samples were analyzed by SEM and AFM: the images observed were reproducible.

3. Results and discussion

3.1. Morphologies by SEM and AFM before treatment

3.1.1. Observation of fractured surface

UPST-N/LPAST-A sample fractured surface was viewed by SEM (Fig. 1) and AFM (Fig. 2) before treatment. SEM and AFM images showed clearly a structure with particles and voids. Nevertheless, these particles were more defined in AFM compared to SEM. With an average size of 60 nm, they were called nanoparticles. They were linked together in aggregates (200 nm) forming a network. The fact that structures are observed without sample treatment is seldom mentioned in the literature [4]. Moreover, nanoparticles of this size have been never reported.

AFM allows to analyze the topography of surfaces, whereas SEM collects secondary electrons up to a given depth (escape depth) and gives information on volume morphology. Consequently, particles definition in AFM in the tapping mode was higher. Besides, AFM in the tapping mode is distinguished by its simplicity and its rapidity to record images. By contrast, SEM suffers from more constraints (vacuum conditions, metal coating of samples) and is destructive.

3.1.2. Comparison of surface and fractured surface

Fig. 3 displays the surface images of the UPST-N/LPAST-A sample. Surface topographies and those of fractured surface (Fig. 2) were similar since we observed nanoparticles, aggregates and networks in both cases. However, nanoparticles were larger on the fractured surface (56 nm) than at the surface (37 nm). This could be explained by a faster and more efficient polymerization due to higher temperature at the surface of the mold.

Samples were smoother (lower roughness) at the surface than on the fractured surface, thus the network, aggregates and nanoparticles were better defined and more visible. We therefore chose to perform AFM analyses of sample surfaces.

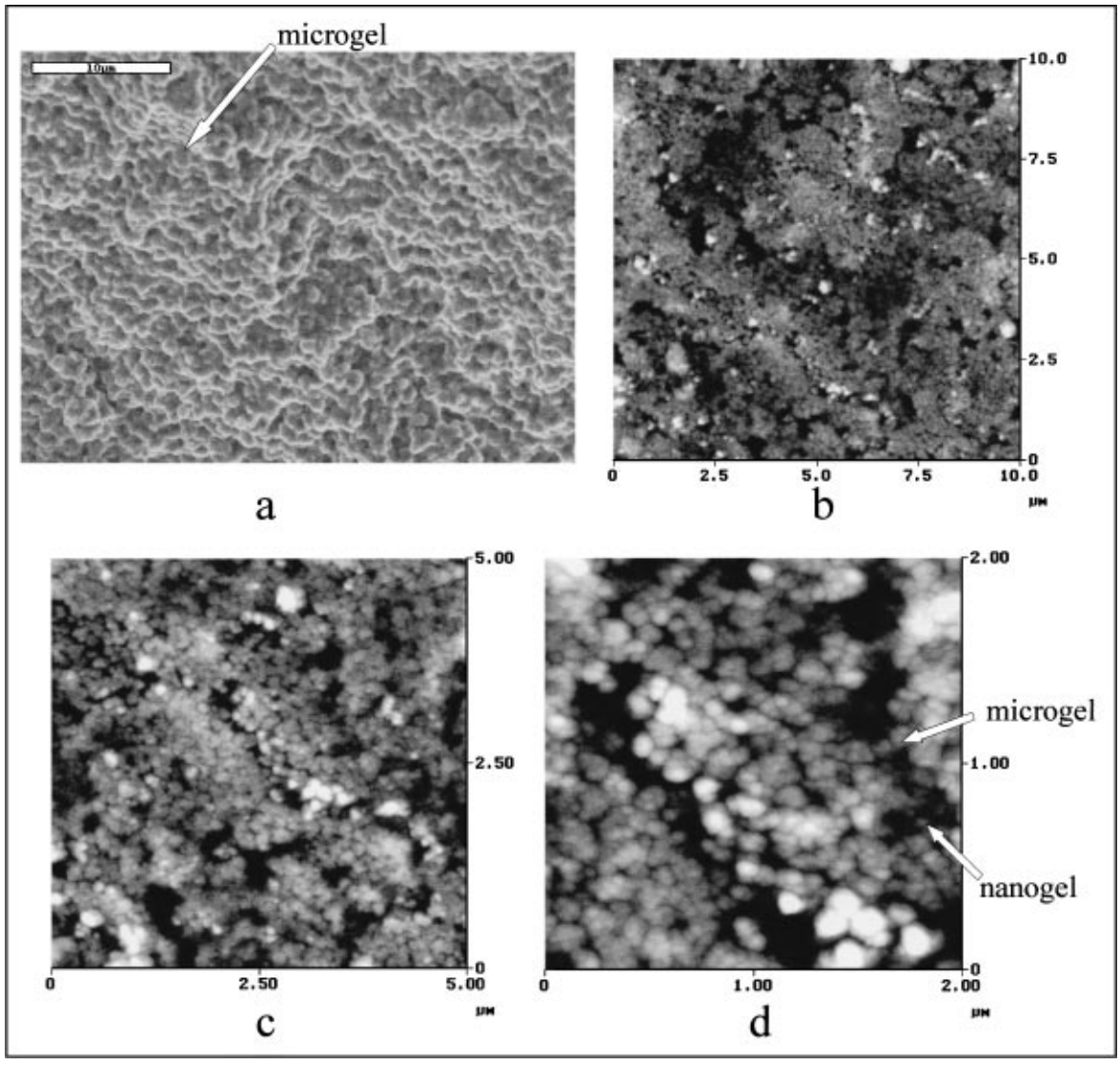

Figure 6 UPST-N/PVAc by SEM and AFM after treatment, (a) fractured surface by SEM, 29 μm × 38 μm (b) surface by AFM, 10 μm × 10 μm, z range = 150 nm (c) surface by AFM, 5 μm × 5 μm, z range = 80 nm (d) surface by AFM, 2 μm × 2 μm, z range = 50 nm.

3.2. Description of morphologies before and after treatment

Treatment solubilizes non-polymerized products. Sample observation before and after treatment investigated the whole morphology and microgel networks respectively. Fractured surface of UPST- P/LPAST-U was observed by SEM before and after treatment (Fig. 4a, b). Fig. 4c, d and Fig. 5 display AFM images of the surface of the same sample at different scales. SEM images differed only slightly before and after treatment, whereas AFM images differed radically.

Treatment reduced nanoparticles and aggregates sizes. Nanoparticles were assumed to be composed of gel particles (crosslinked UP/ST molecules) containing a LPA phase: removal of LPA yielded gel particles, which were thinner than the nanoparticles. Nanoparticles were particles observed before treatment whereas only gel particles were observed after treatment. In accordance with the literature [4, 15, 20], gel nanometrical particles were called nanogels and their aggregates microgels. Treatment transformed nanoparticles into nanogels and aggregates into microgels and also modified the network of microgels. All microgels were brought together into compact regions, creating much void (compare Fig. 4c, d).

To our knowledge, the existence of nanogels and nanoparticles has never been reported in the literature, although microgels are generally observed [3, 4, 6, 9, 12]. These observations in particular concerned miscible blends with PVAc. In order to compare our observations with the literature, we examined another cured blend sample based on UPST-N/PVAc in a weight proportion of 69 : 30. SEM and AFM observations after treatment are presented in Fig. 6a, b. Microgels with an average size of 600 nm were only observed by SEM on fractured surface (Fig. 6a). AFM images of surface (Fig. 6b–d) were recorded at different sizes ($10 \times 10\ \mu m^2$, $5 \times 5\ \mu m^2$, $2 \times 2\ \mu m^2$). Nanogels with an average size of 55 nm and microgels with an average size of 180 nm were visible. Whatever UPST/LPAST blends, particles with nanometrical sizes were identified by AFM in the tapping mode.

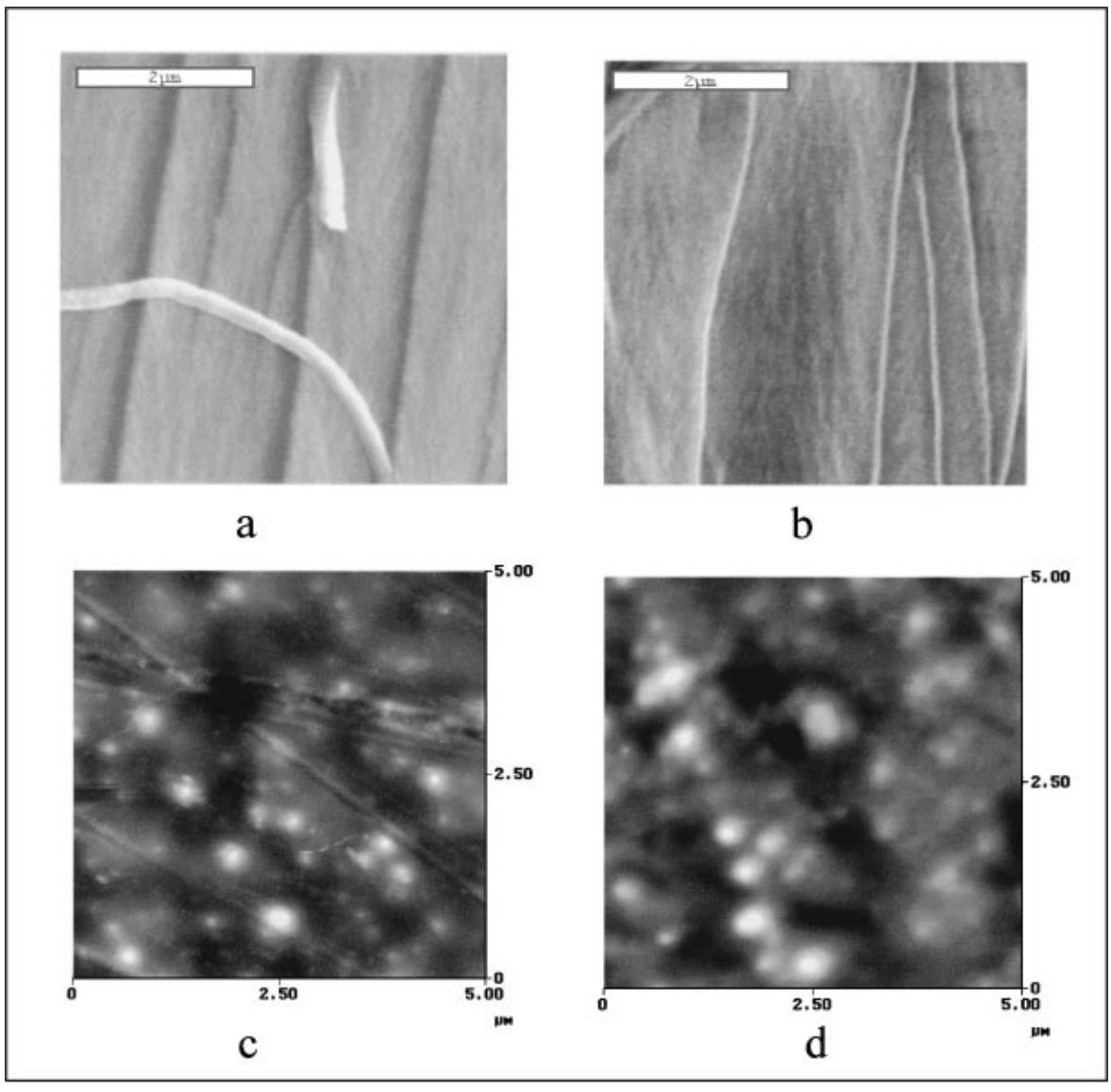

Figure 7 Neat cured resins by SEM and AFM, UPST-N resin (a) fractured surface by SEM, 5 μm × 5 μm (c) surfaces by AFM, 5 μm × 5 μm, z range = 80 nm; UPST-P resin (b) fractured surface by SEM, 5 μm × 5 μm (d) surface by AFM, 5 μm × 5 μm, z range = 80 nm.

3.3. Morphologies of the four cured UPST/LPAST blends

The two unsaturated polyester resins (UPST-N and UPST-P) were imaged by SEM and AFM (Fig. 7). As reported in the literature [6], SEM images (Fig. 7a, b) were characterized by an oriented continuous structure. No microgel was identifiable. Many tiny particles appeared on the surface as observed by AFM (Fig. 7c, d).

The four cured blends were investigated by AFM and SEM (not shown here) before and after treatment. Figs 5, 8, 9, 10 present $2 \times 2\ \mu m^2$ and $10 \times 10\ \mu m^2$ AFM images of the surfaces. All images showed a network of nanoparticles and aggregates before treatment, and nanogels and microgels after treatment. However, whole networks differed from one blend to another with more or less numerous and more or less expanded voids and larger or smaller particles.

In order to compare these four systems, the sizes of all particles before and after treatment were measured (see Table III). The volume shrinkage and the void volume were evaluated to estimate the aptitude to compensate for the polymerization shrinkage (Table IV). The influence of the nature of UP and LPA on the cured morphology can be shown (Table III and Figs 5, 8, 9, 10). Nanoparticle sizes varied from 37 to 57 nm, whereas aggregate sizes varied from 146 to 231 nm. Aggregates were smaller for UPST-N/LPAST-U (Fig. 8a, c) than UPST-P/LPAST-U (Fig. 5a, c). The presence of NPG enhanced the solubilityof UPST-N in styrene [6]. Aggregates for UPST-N/LPAST-A (Fig. 10a, c) were smaller than for UPST-N/LPAST-U (Fig. 8a, c). The same observation was valid for the

TABLE III Average sizes and their standard deviations (nm) of nanoparticles, aggregates, nanogels and microgels observed by AFM

	Before solubilization		After solubilization	
	nanogel size (nm) (st. dev.)	microgel size (nm) (st. dev.)	nanogel size (nm) (st. dev.)	microgel size (nm) (st. dev.)
UPST-N/LPAST-U	46 (7)	167 (16)	43 (3)	146 (19)
UPST-N/LPAST-A	37 (4)	146 (21)	20 (4)	80 (9)
UPST-P/LPAST-U	57 (6)	231 (17)	46 (4)	212 (21)
UPST-P/LPAST-A	44 (7)	139 (17)	39 (2)	123 (12)

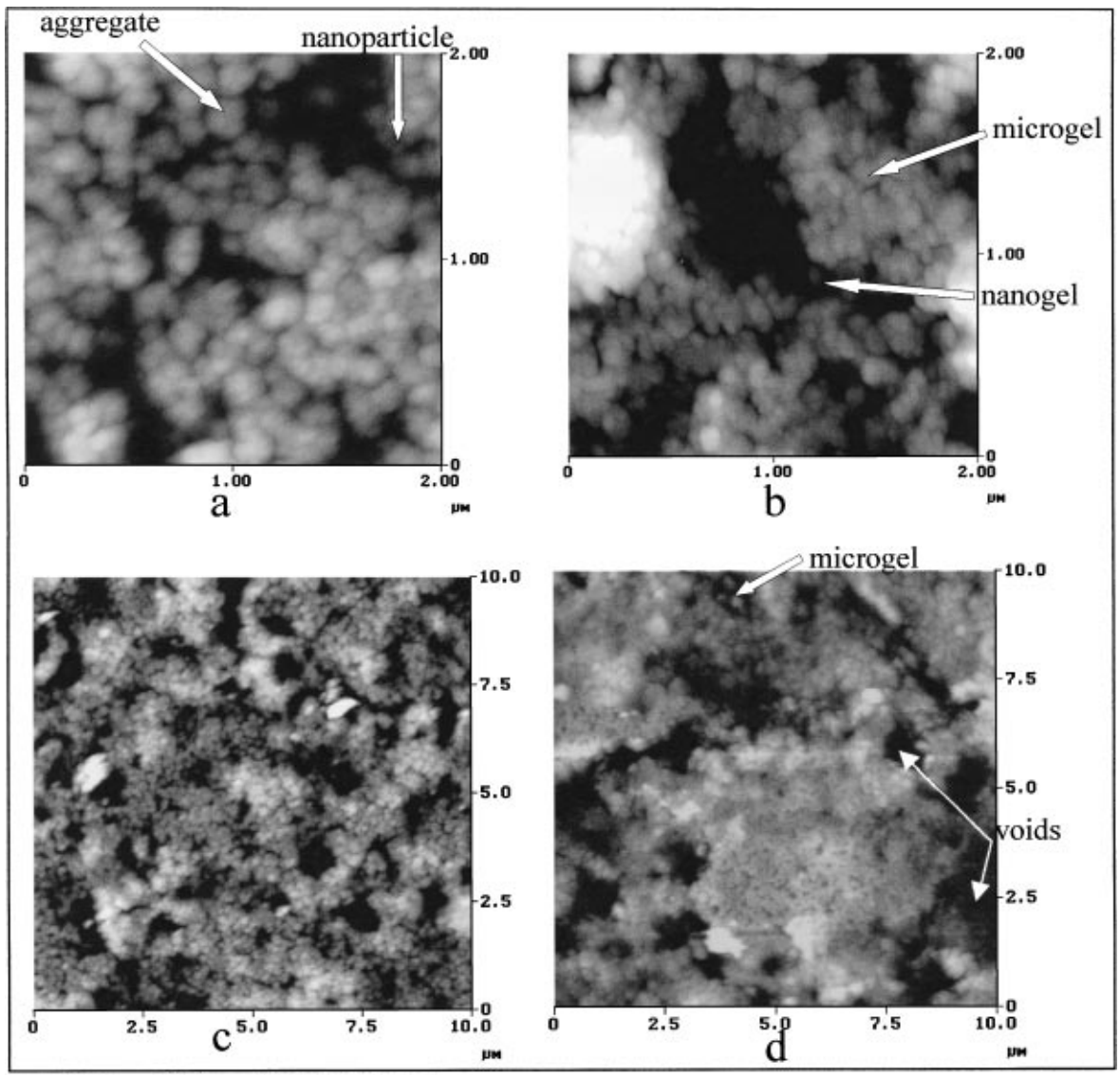

Figure 8 UPST-N/LPAST-U surfaces by AFM, before treatment (a) 2 μm × 2 μm, z range = 80 nm (c) 10 μm × 10 μm, z range = 80 nm; after treatment (b) 2 μm × 2 μm, z range = 100 nm (d) 10 μm × 10 μm, z range = 100 nm.

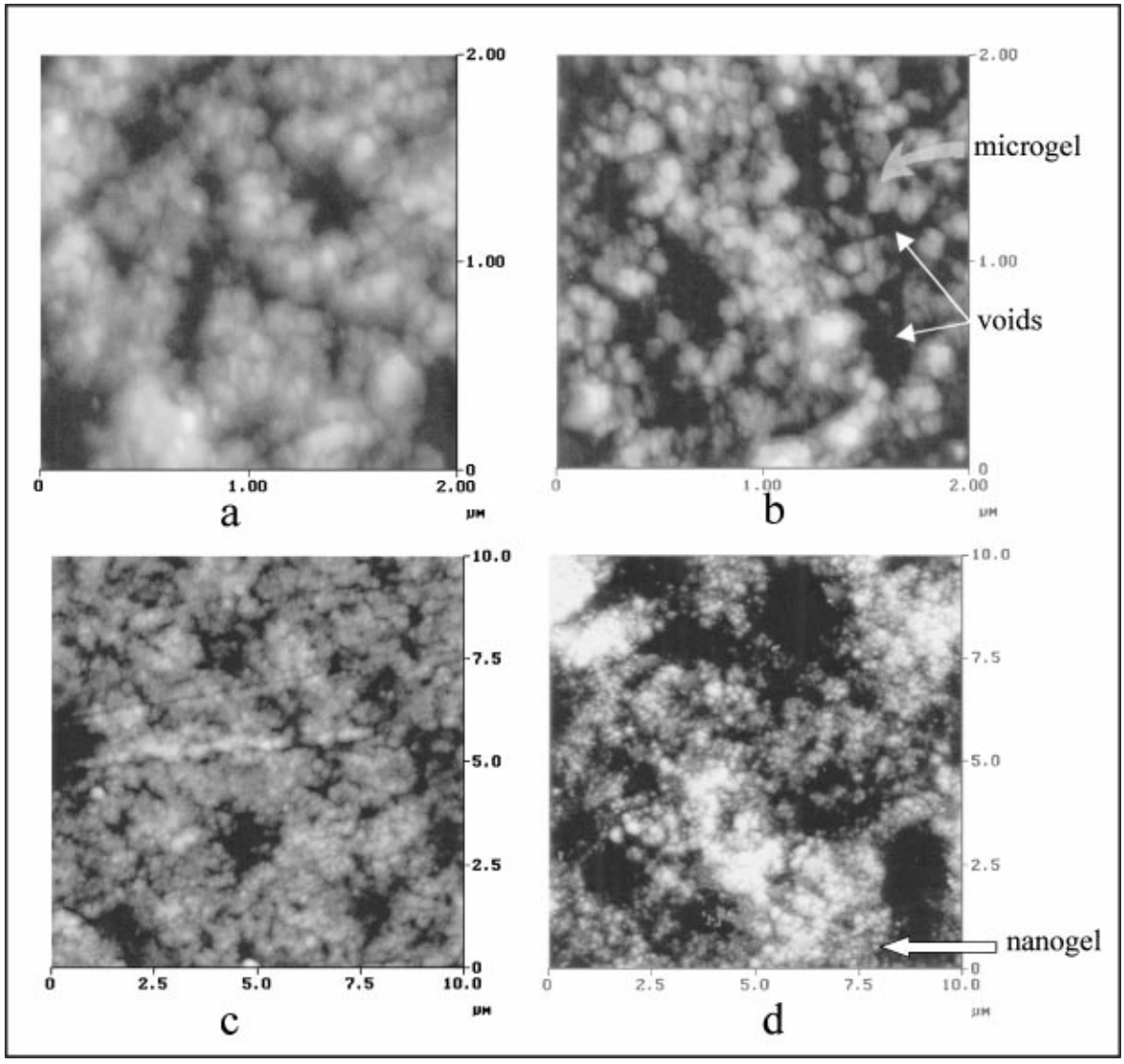

Figure 9 UPST-P/LPAST-A surfaces by AFM, before treatment (a) 2 μm $\times$ 2 μm, z range = 50 nm (c) 10 μm $\times$ 10 μm, z range = 80 nm; after treatment (c) 2 μm $\times$ 2 μm, z range = 50 nm (d) 10 μm $\times$ 10 μm, z range = 80 nm.

TABLE IV Visual appearances, volume shrinkages (%) and void volumes (%) of UPST/LPAPST blends. The average values and their standard deviations are indicated

	Visual appearance	Volume shrinkage (%) (st. dev.)	Void volume (%) (st. dev.)
UPST-N/LPAST-U	white opaque	6.0 (0.2)	5.2 (0.1)
UPST-N/LPAST-A	cloudy, translucent	7.4 (0.2)	3.9 (0.3)
UPST-P/LPAST-U	white opaque	6.2 (0.2)	5.5 (0.2)
UPST-P/LPAST-A	cloudy, translucent	8.4 (0.2)	3.8 (0.1)

UPST-P/LPAST-A (Fig. 9a, c) and UPST-P/LPAST-U systems (Fig. 5a, c). LPAST-U contained urethane functions, which are known to enhance the dipole moment and decrease miscibility between LPAST-U and UPST-N (or UPST-P) [6]: LPAST-U was less soluble than LPAST-A in UPST-N (or UPST-P). Particle sizes were influenced by competition between the polymerization kinetic and the phase separation rate. With high miscibility between UPST and LPAST, numerous small particles were generated during curing. On the other hand, when phase separation appeared earlier (worse miscibility), fewer but bigger particles were formed (Fig. 5) [5, 6]. In order to obtain whole networks constituted by small particles (nanoparticles, aggregates) UPST and LPAST must be highly miscible [7]. Microgels were small for all the cured blends (average size: 140 nm) compared to the literature [2, 4, 6, 7, 15], indicating that used blends UPST/LPAST were very miscible. Treatment resulted in the size reduction of aggregates and nanoparticles. Particle sizes were notably reduced for UPST-N/LPAST-A (Fig. 10b, d) with much of the LPA phase included inside particles. This confirmed that UPST-N and LPAST-A were highly miscible [6]. With this system, phase separation appeared very late on (Fig. 10).

After curing, samples presented different light opacity, the volume shrinkage varied from 6.0% to 8.4% and void volume as measured by AFM analysis varied from 3.8 to 5.5% (Table IV). Samples with low shrinkages corresponded to opaque samples with large void volumes (UPST-N/LPAST-U and UPST- P/LPAST-U). In contrast, samples with elevated shrinkages were cloudy and translucent and exhibited low void volumes (UPST-N/LPAST-A and UPST-P/LPAST-A). Light opacity

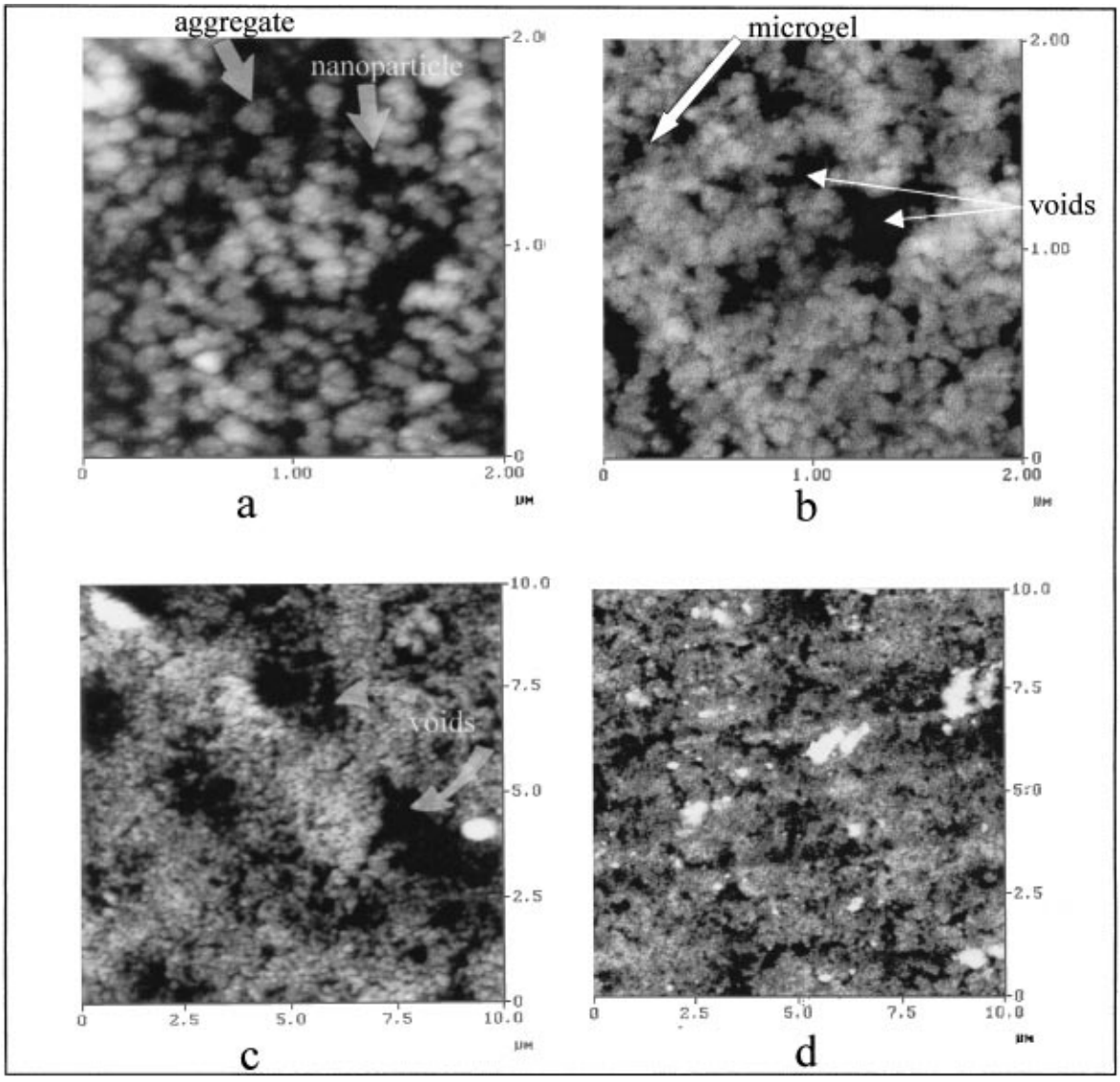

Figure 10 UPST-N/LPAST-A surfaces by AFM, before treatment (a) 2 μm × 2 μm, z range = 50 nm (c) 10 μm × 10 μm, z range = 80 nm, after treatment (b) 2 μm × 2 μm, z range = 80 nm (d) 10 μm × 10 μm, z range = 100 nm.

was used as a first indication of the states of aggregate networks. Systems with LPAST-A had higher volume shrinkage than systems containing LPAST-U. LPAST-A was therefore less effective than LPAST-U in compensating for shrinkage. Aggregate sizes (Table III) were closely correlated with void volumes (Table IV). Smaller aggregates yielded smaller void volumes.

4. Conclusion

Atomic Force Microscopy (AFM) in the tapping mode was a powerful tool to study the morphology of cured samples of miscible systems UP/LPA/ST. Besides aggregates and microgels previously observed by Scanning Electron Microscopy (SEM) smaller particles, nanoparticles and nanogels (with sizes varying from 20 to 57 nm), were identified in the present work by AFM. AFM conditions were simple and images were visible with nanometric resolution. Generally SEM is performed on fractured surfaces to investigate morphology. AFM was performed on fractured surfaces and surfaces: results revealed the same morphology, with smaller particles at the surface. AFM images were recorded at the surface, this being easier.

Samples were examined without LPA solubilization, though this is seldom reported in the literature. Nanoparticles were observed and were linked together in aggregates. After LPA extraction, nanogels constituting microgels were observed (140 to 300 nm).

Examination of all samples indicated that the miscibility between UPST and LPAST was a key parameter to help to explain the morphology of the whole network. Higher miscibilities resulted in more numerous nanogels, and smaller microgels. A relation between the microgel sizes and the void volumes was established.

The capability of AFM to image UP/LPA/ST cured system being demonstrated, the investigation of the cure steps and morphologies of others blends must be very informative.

Acknowledgment

The authors wish to thank Annie Richard for the SEM images.

References

1. T. MITANI, H. SHIRAISHI, K. HONDA and G. E. OWEN, 44th Annual Conference, Composites Institute, The Society of the Plastics Industry (1989), Session 12-F.

2. W. LI and J. LEE, *Polymer* **39** (1998) 23.
3. Y. J. HUANG and C. C. SU, *ibid.* **35** (1994) 2397.
4. *Idem., J. Appl. Polym. Sci.* **55** (1995) 323.
5. Y. J. HUANG and C. M. LIANG, *Polymer* **37** (1996) 412.
6. Y. J. HUANG and W. C. JIANG, *ibid.* **39** (1998) 6631.
7. Y. J. HUANG and J. C. HORNG, *ibid.* **39** (1998) 3683.
8. C. B. BUCKNALL, P. DAVIES and I. K. PARTRIDGE, *ibid.* **26** (1985) 109.
9. C. B. BUCKNALL, I. K. PARTRIDGE and M. J. PHILIPPS, *ibid.* **32** (1991) 636.
10. J. C. LUCAS, J. BORRAJO and J. J. WILLIAMS, *ibid.* **34** (1993) 1886.
11. M. KINKELAAR, B. WANG and L. J. LEE, *ibid.* **35** (1994) 3011.
12. V. A. PATTISON, R. R HINDERSINN and W. T. SCHWARTZ, *J. App. Polym. Sci.* **18** (1974) 2763.
13. J. P. LECOINTE, J. P. PASCAULT, L. SUSPENE and S. YANG, *Polymer* **33** (1992) 3226.
14. C. P. HSU and L. J. LEE, *ibid.* **32** (1991) 2263.
15. Y. S. YANG and L. J. LEE, *ibid.* **29** (1988) 1793.
16. L. R. ROSS, S. P. HARDEBECK and M. A. BACHMANN, 43rd Annual Conference, Composites Institute, The Society of the Plastics Industry (1988) Session 17-C.
17. I. REYNAUD-LAPORTE, M. VAYER, J. P. KAUFFMANN and R. ERRE, *Corrosion Science* **8** (1997) 175.
18. J. H. BUTLER, D. C. JOY, G. F. BRADLEY and S. J. KRAUSE, *Polymer* **36** (1995) 1781.
19. C. SERRE, M. VAYER, C. OLLIVE and R. ERRE, *J. Mat. Sci.* **34** (1999) 4203.
20. W. FUNKE, O. OKAY and B. JOOS-MÜLLER, *Advances in Polymer Science* **136** (1998) 139.

Received 14 October 1999
and accepted 16 May 2000